# Mount Harper Volcanic Complex, Ogilvie Mountains: A far-flung occurrence of the Franklin Igneous Event?

***Grant M. Cox***[1]
*McGill University, Montreal, Quebec, Canada*

***Charles F. Roots***
*Geological Survey of Canada, co-located at Yukon Geological Survey, Whitehorse, Yukon*

***Galen P. Halverson, William G. Minarik***
*McGill University, Montreal, Quebec, Canada*

***Francis A. Macdonald***
*Harvard University, Massachusetts, U.S.A.*

***Lucie Hubert-Theou***
*McGill University, Montreal, Quebec, Canada*

Cox, G.M., Roots, C.F., Halverson, G.P., Minarik, W.G., Macdonald, F.A., and Hubert-Theou, L., 2013. Mount Harper Volcanic Complex, Ogilvie Mountains: A far-flung occurrence of the Franklin Igneous Event. *In:* Yukon Exploration and Geology 2012, K.E. MacFarlane, M.G. Nordling, and P.J. Sack (eds.), Yukon Geological Survey, p. 19-36.

## ABSTRACT

The middle Neoproterozoic (717 Ma) Mount Harper Volcanic Complex (MHVC) is a calc-alkaline magmatic suite developed within a rift system on the northwestern margin of Laurentia. Based on its low $Al_2O_3$, $Na_2O$, and $TiO_2$ contents, the primary melt was derived from a harzburgitic source, was most likely picritic in composition, and required mantle potential temperatures above those recognized for the ambient mantle. Constraints on mantle melting place the mantle at ~6 km, a depth that would require significant crustal attenuation.

Although the volcanic rocks at Mount Harper are the same age as the Franklin Large Igneous Province, the geochemical trends are distinct. Apart from their age, the only plausible link would be to consider the MHVC as the product of a partial melt at the margin of a dispersed mantle plume.

[1]*grant.cox@mail.mcgill.ca*

## INTRODUCTION

Age constraints on Cryogenian volcanism within the Canadian Cordillera indicate that magmatic events are restricted to two principal episodes: the ~780 Ma Gunbarrel Event (Harlan *et al.*, 2003) and the ~720 Ma Franklin Igneous Event (Denyszyn *et al.*, 2009; Heaman *et al.*, 1992). Both of these events produced radiating dike swarms in northern Laurentia. Radiating dikes may represent the physical manifestation of mantle plumes and are often associated with Large Igneous Provinces (LIP) (Ernst and Buchan, 1997, 2001, 2003), although the association of radiating dikes to plumes is contested (McHone *et al.*, 2005). This LIP-plume connection may be a precursor to continental breakup, suggesting that LIP's play an important role in this process (Dalziel *et al.*, 2000; Hill, 1991; Li *et al.*, 2003; Storey, 1995).

The Mount Harper Volcanic Complex (MHVC) consists of basalt to rhyolite which erupted into a half-graben on the broad platform flanking the west side (present coordinates) of Laurentia. Up to 1600 m of lava flows and breccias are preserved and are overlain by diamictite, tuff, and other sediments of the Rapitan Group (Sturtian glaciation). This study was aimed at understanding the evolution of rifted margins using the chemistry of the volcanic rocks to determine the composition of the source magma, its temperature, and the nature of the decompressing mantle. These constraints can then be used to place limits on crustal and lithospheric thicknesses and, by implication, their tectonic setting.

In this paper, new and previously published major element geochemical data are combined for the MHVC, predominantly from the lower ~900 m of basaltic volcanics. A thermodynamic melt model is applied to establish basic constraints on the evolution of the MHVC. These results elucidate the mantle melting regime and place constraints on the thickness of the overlying crust. The MHVC is then compared to the coeval Natkusiak basalts (Victoria Island, Nunavut) which forms a part of the Franklin Igneous Event, attempting to ascertain whether the MHVC could represent a distant manifestation of this magmatic episode.

## GEOLOGIC SETTING OF THE MOUNT HARPER VOLCANIC COMPLEX

Mount Harper, 70 km north of Dawson (Fig. 1a,b), is surrounded by 105 km$^2$ of predominantly sub-aqueous mafic to intermediate volcanic rock with volumetrically minor rhyolite. The mountainous terrain affords clear observation of its nearly conformable attitude atop a shallow marine sedimentary sequence (Mustard and Roots, 1997). The Mount Harper Volcanic Complex (MHVC) sits para-conformably on an alluvial fan wedge (Lower Mount Harper Group) which in turn sits atop the Callison Lake dolostone (Fig. 1b,c), a dominantly carbonate unit with interbedded shales that contain sedimentary talc (Tosca *et al.*, 2011). Different interpretations of the age and sedimentary regime of the Callison Lake dolostone have led to its proposed assignment to 1) the underlying Fifteenmile Group (Thompson *et al.*, 1987), 2) the overlying Mount Harper Group (Macdonald *et al.*, 2011), but is now recognized as 3) a distinct unit, possibly a correlative of the Coates Lake Group in the Mackenzie Mountains (NWT) (Macdonald *et al.*, 2012).

Five kilometres east of Mount Harper, the Lower Mount Harper Group comprises up to 1100 m of mainly conglomerate with interbedded sandstone and red calcareous mudstone. These coarse epiclastic sediments were deposited north of the steeply-dipping syn-sedimentary and syn-volcanic Harper fault (Fig. 1b), partly filling an east-trending half-graben (Mustard and Roots, 1997). The Lower Mount Harper Group thins rapidly to the north, where it transitions into sandstone and mud-cracked siltstones and mudstones of presumed lacustrine affinity (Mustard, 1991; Mustard and Donaldson, 1990; Mustard and Roots, 1997). It is overlain conformably by ~900 m of sub-aqueously extruded basalt flows, which suggests that the MHVC was deposited in a rapidly subsiding basin.

The MHVC is bounded above by glaciogenic diamictite of the Rapitan Group. In a rhyolite flow in the upper Mount Harper Group and in a tuff within the diamictite, radiometric ages on zircons fix the age of this contact at 717 Ma (Macdonald *et al.*, 2010).

## MOUNT HARPER VOLCANIC COMPLEX

Roots (1987) and Mustard and Roots (1997) divided the MHVC into six informal units (members A through F; Figs. 1b and 2) based on stratigraphic observations and geochemistry. Members A and B are dominated by pillowed (Fig. 3a) and massive flows, with common chloritic and hematitic alteration. The occurrence of pahoehoe flow textures near the top of member B indicate a sub-aerial eruptive phase in an otherwise dominantly sub-aqueous eruptive sequence. Member C is a lithologic

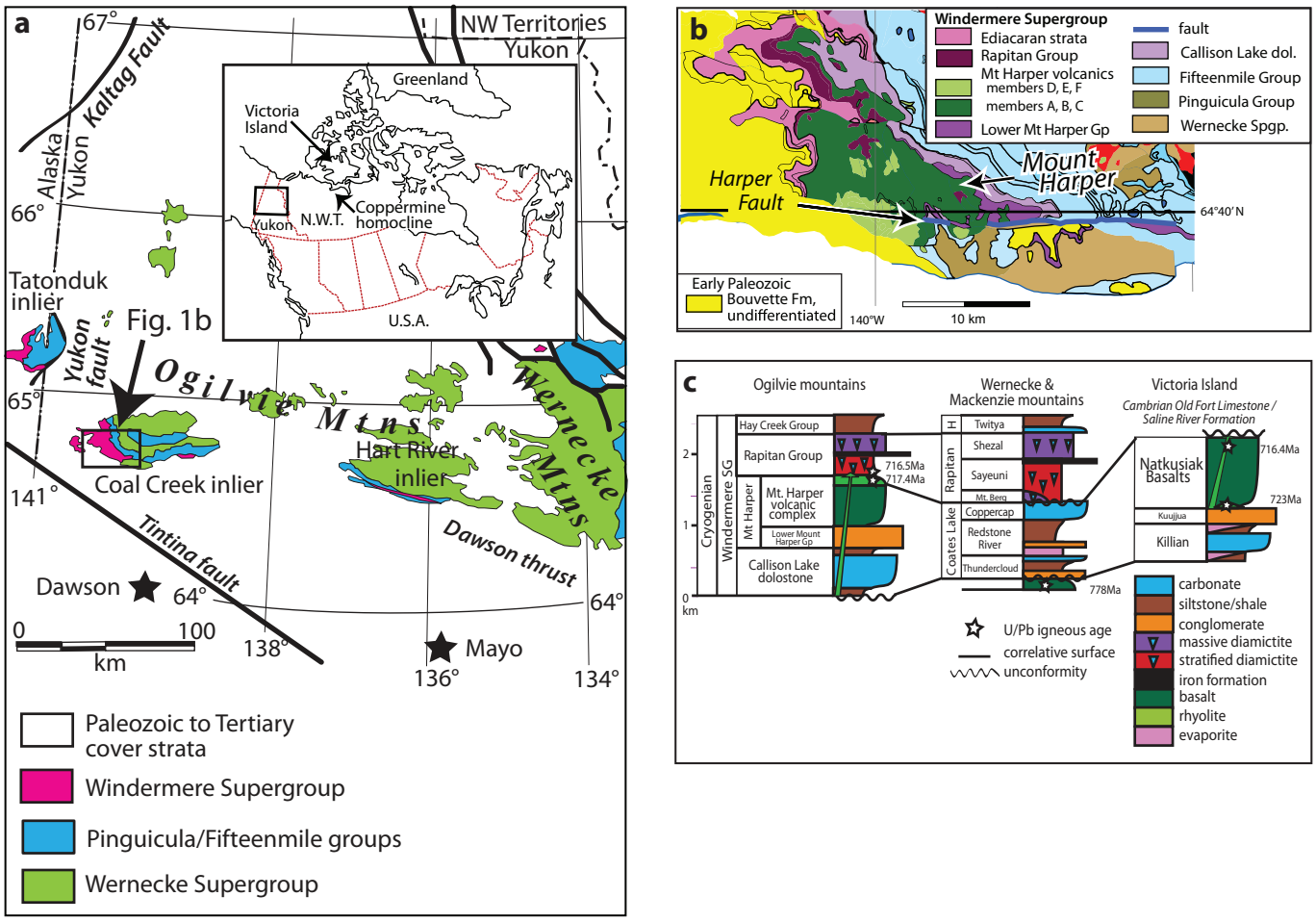


***Figure 1.*** *(a) Regional map for Yukon, NWT, and Alaska; (b) distribution of members of the Mount Harper Volcanic Complex and enclosing units; and (c) stratigraphic column showing stratigraphic correlations with the Wernecke Mountains and Victoria Island (from Macdonald et al., 2012).*

unit: a stratigraphic interval composed almost entirely of sub-aqueous volcanic breccia and tuff that represents a period of explosive volcanism as well as erosional destruction of the member A and B volcanic edifice (Mustard and Roots, 1997). Member D comprises rhyolite flows and domes (Fig. 3b), subsequently partly eroded and succeeded by pillowed and massive andesite flows of member E and then by sub-aqueous basaltic andesite to andesite flows of member F. Mustard and Roots (1997) argued that some lavas in member D were sub-aerial, but definitive evidence is absent.

The original size and extent of the MHVC cannot be ascertained because it is dissected by faults and eroded, including scouring by mid-Cryogenian glaciation. Nevertheless, remnants of the MHVC extend laterally across ~17 km of the Coal Creek inlier (Fig. 1a) and reach a maximum continuous thickness of ~900 m. A composite log of Members A through F (Fig. 2) suggests that the original volcanic edifice was at least ~1600 m thick. Beyond the Coal Creek inlier, volcanic flows at a similar stratigraphic level occur within the Tatonduk and Hart River inliers (Fig. 1a), indicating that the original volcanic field was possibly more extensive.

## AGE CONSTRAINTS

The age of the rhyolitic member D is well constrained by a U-Pb zircon age of 717.43±0.14 Ma (Macdonald *et al.*, 2010). A rhyolitic tuff near the base of Rapitan glacial diamictite atop the edifice composed of members

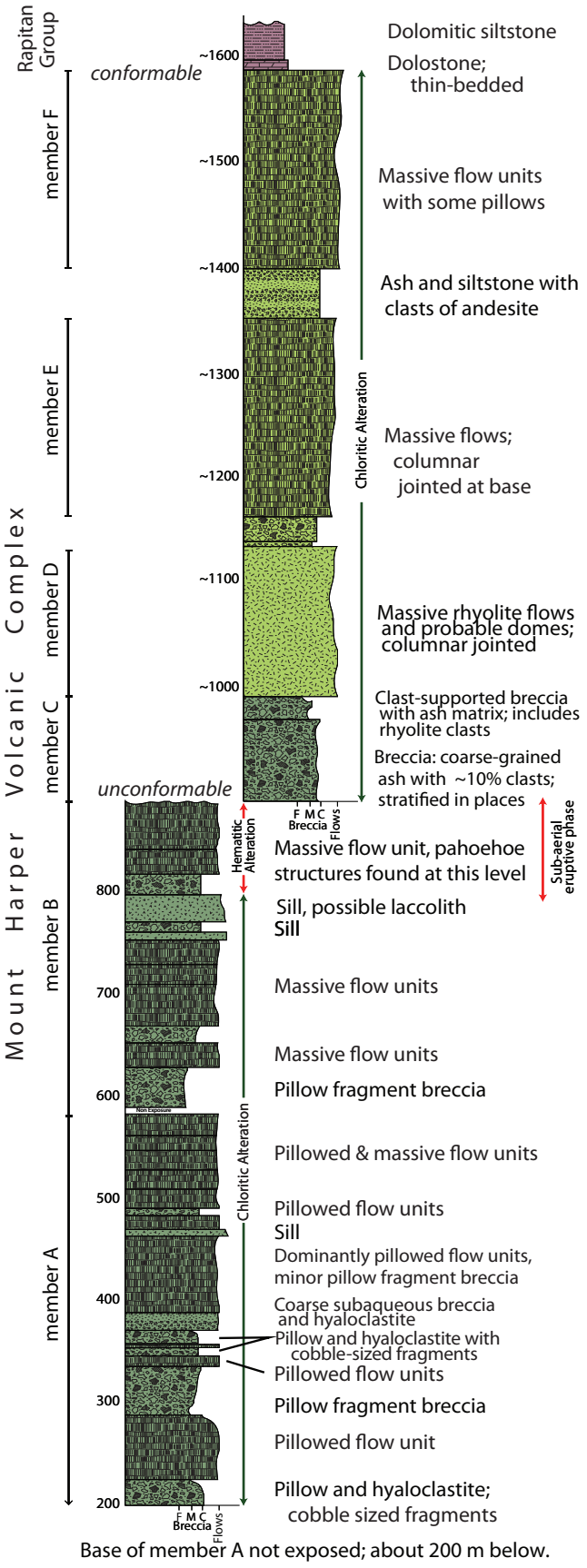


A and B yielded a U-Pb zircon age of 716.47±0.24 Ma (Macdonald *et al.* 2010). This tuff indicates that the initial phase of volcanism was pre- or syn-glacial.

The apparently conformable contacts between members D through F imply that these eruptive phases were continuous. However, the extensive erosional contact separating members A and B from member D may represent a significant time gap between volcanic events. As discussed below, the geochemical characteristics of Member F suggests a return to the melting regime characterized by members A and B. The entire volcanic sequence was therefore most likely erupted during a single magmatic cycle.

## ALTERATION

Due to the greenschist facies alteration of these rocks (chlorite and sericite alteration assemblage), many of the rocks are highly hydrated, in particular those of mafic to intermediate compositions. Loss on ignition (LOI) in some samples can be greater than 10%, in which mobile elements such as Ca and Na have been significantly affected. Table S1 (Appendix 1) reports major element data only from rocks with less than 5% LOI; alteration effects are not apparent with no correlation between major element abundances and LOI.

## PETROGRAPHY

### MEMBERS A AND B

Flows in members A and B contain (micro)phenocrysts of olivine that are pseudomorphed by chlorite. Clinopyroxene (CPX) is abundant along with needles of plagioclase that forms a dense groundmass mesh often containing Fe-Ti oxides. Orthopyroxene (OPX) is absent. An original glassy groundmass is now entirely altered to chlorite±feldspar±sericite. Unlike A, which is chloritic-altered, stratigraphically higher flows of member B are extensively altered to hematite. This zone of hematite

***Figure 2.*** *Composite stratigraphic log of the MHVC. Member B, and possibly member A, were partly eroded before eruption and deposition of members D, E, and F; ~900 m are preserved. Physical volcanic features are described by Roots (1987) and Mustard and Roots (1997).*

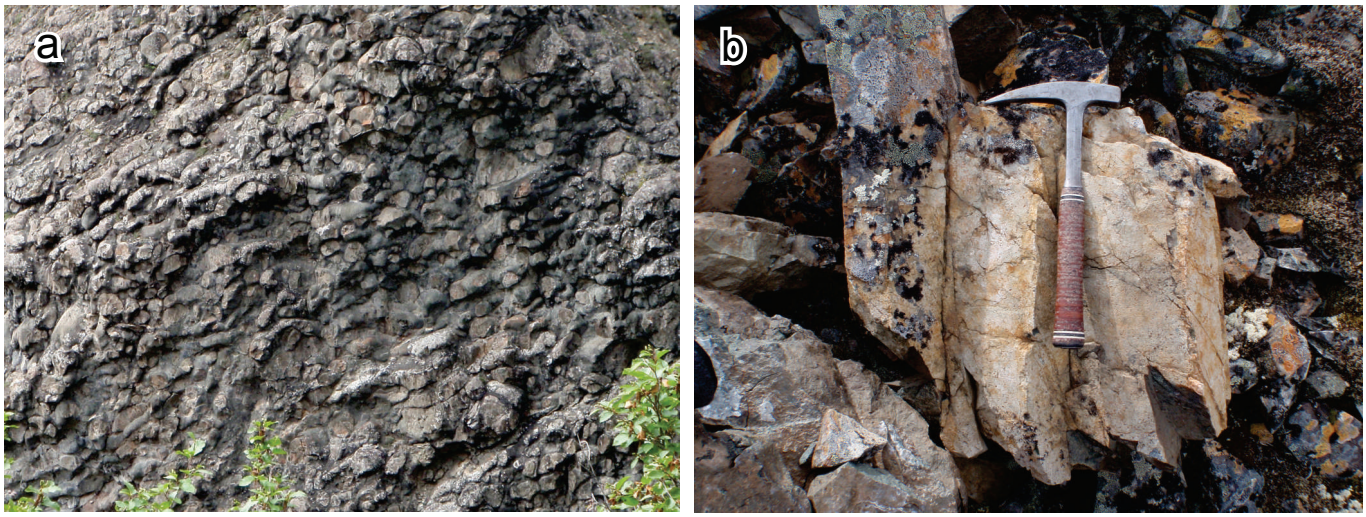


***Figure 3.*** *(a) Cliff face, about 10 m high, exposes rounded pillows in member A (64°40.0'N and 139°54'W; 2 km SW of Mount Harper); (b) columnar rhyolite of member D weathers into conical rubble hills 6.5 km west of Mount Harper.*

alteration coincides with the appearance of pahoehoe flow structures, suggesting that this alteration may be a primary feature related to sub-aerial eruption. The general crystallization sequence for members A and B was likely olivine » clinopyroxene » plagioclase » glass.

### MEMBER D

Phenocrystic K-feldspar and plagioclase, commonly saussuritized, are the dominant mineral phases for member D. Minor phases include titanite (I- type index mineral; Chappell and White, 2001), Fe-Ti oxides and zircon, with xenocrystic garnet (Mustard and Roots, 1997; Roots, 1987). An original glassy groundmass is entirely altered to quartz ± sericite ± feldspar.

### MEMBER E

The flows are extensively crystallized, plagioclase and minor clinopyroxene being easily distinguishable phases. The groundmass phases include quartz plus Fe-Ti oxides. Olivine is absent.

### MEMBER F

Flows are locally seriate and plagioclase-phyric, with visible augite. Voids, into which plagioclase laths project, are filled with secondary silica. The largely indistinguishable groundmass was most likely glass but now contains quartz ± sericite ± feldspar alteration phases. Alteration indicated by chlorite and other clay minerals is extensive.

## GEOCHEMICAL CHARACTERISTICS OF MHVC

Major element Harker and Fenner diagrams (Fig. 4) along with alkali vs. silica plots show distinctive geochemical groupings and trends. Members A and B are characterized as basalts to basaltic andesites, member D as rhyolites and both members E and F are andesites but with significantly different bulk compositions (Fig. 4a).

### MEMBERS A AND B

While members A and B are defined stratigraphically, they both fall on a compositional trend from basalt to basaltic andesite, with the most primitive examples having MgO contents of ~12%. The combination of low $TiO_2$, low $Al_2O_3$, and low $Na_2O$ in these rocks suggests either a depleted mantle source or extensive melting of a fertile source. The liquid line of descent for members A and B is consistent with the fractionation of olivine ± clinopyroxene, and the delay of plagioclase crystallization. A lack of FeO and $TiO_2$ enrichment with decreasing MgO is consistent with calc-alkaline magmatism.

### MEMBER D

Member D reflects a switch from mafic to felsic magmatism within the evolution of the MHVC. These rhyolites are characterized by 70-78% $SiO_2$ with no intermediate compositions that link them via a liquid line of descent to the extrusion of lower members A and B. Aluminium saturation ratios ($Al_2O_3/[CaO+K_2O+Na_2O]$)

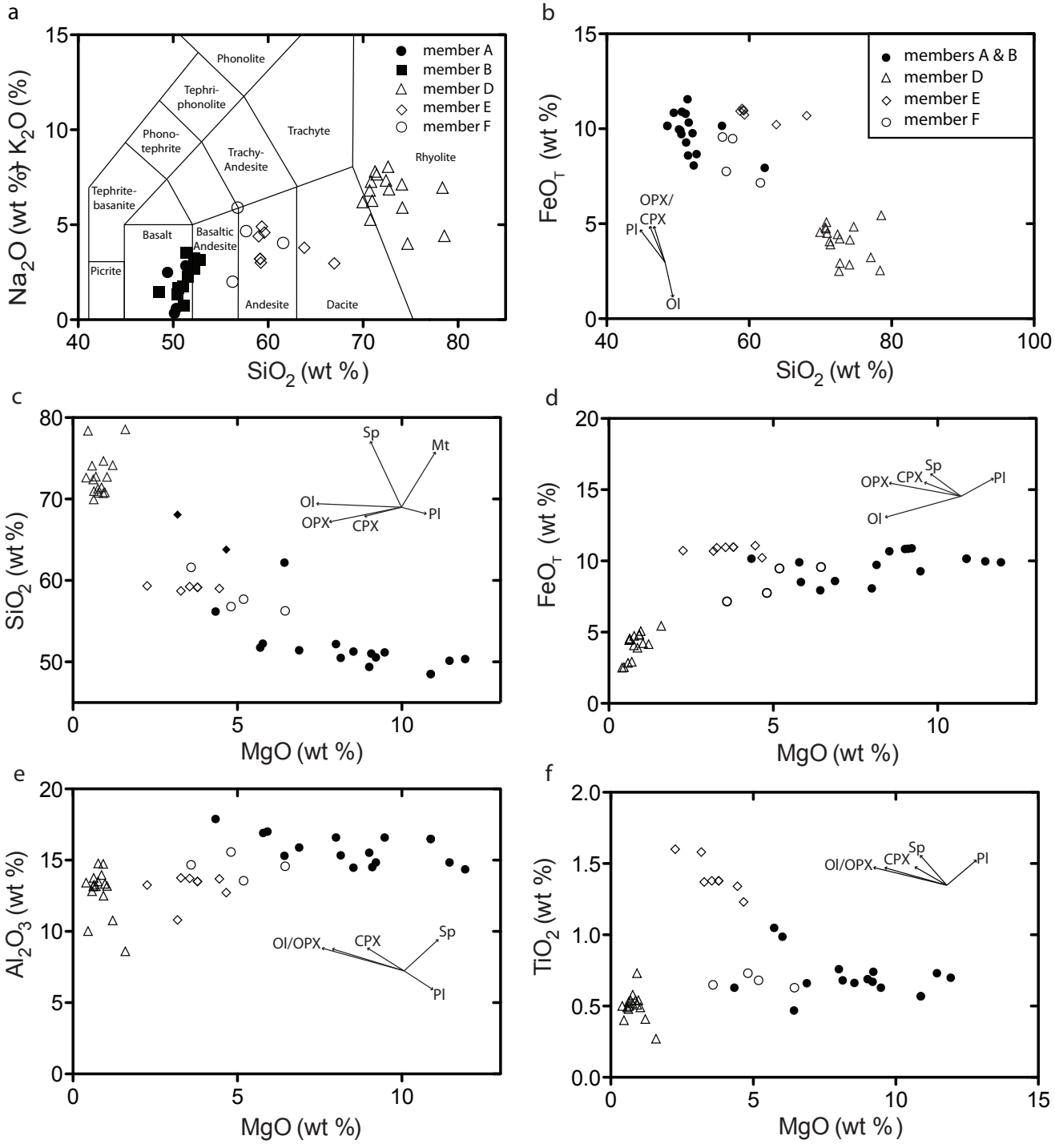


***Figure 4.*** *Major element plots show the distinctive geochemical evolution of the MHVC. Particularly apparent on the Harker diagrams ($SiO_2$ on the x-axis) is the distinctive geochemical trend represented by members A and B. A silica gap of ~15% (i.e., the "Daly" gap) separates members A and B from the rhyolitic member D. On the Fenner diagrams (MgO on x-axis) members A, B and F define a liquid line of descent characteristic of delayed plagioclase crystallization. Member E lavas are distinct from the mafic to intermediate lavas of members A, B, and F; note the trend to increasing TiO2 and constant FeO. Radiating arrows indicate possible trends resulting from crystallization of normative minerals: CPX – clinopyroxene; Mt – magnetite; Ol - olivine; OPX – orthopyroxene; Pl – plagioclase; Sp - spinel.*

range from metaluminous to peraluminous (0.84 to 1.44) along with normative corundum. However, the occurrence of titanite in the mineral assemblage precludes simple classification as either I or S-type rhyolites (Chappell and White, 2001). Normative compositions projected into the Qz-Ab-Or-$H_2O$ system (Blundy and Cashman, 2001) reveal the dominant role of low pressure polybaric fractionation of albite towards $K_2O$ and $SiO_2$-rich compositions (Fig. 5).

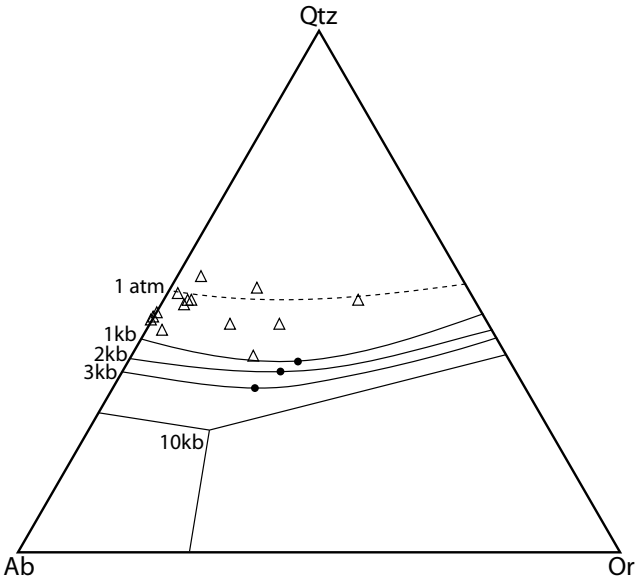


***Figure 5.*** *Projection of the normative composition of member D rhyolites following the method outlined by Blundy and Cashman (2001). This projection reveals a trend of polybaric crystallization dominated by the fractionation of plagioclase. Black dots are the water saturated minimums. Water undersaturation and decreasing pressure move these minimums towards the Qtz-Or join.*

### MEMBER E

Member E lavas are andesitic to dacitic but plot well away from the fractionation trend observed in members A and B (Fig. 4f). The major element liquid line of descent for member E is complicated but most likely associated with the fractionation of a gabbroic assemblage (Pl+CPX±Sp). The intermediate nature of member E, coupled with the immediate precursor eruption of rhyolites, possibly indicates the role of magma mixing between a residual member D liquid and a new influx of mafic magma. Simple mixing between members A and B and member D compositions would require that the member D contribution be ~30-40% to achieve the approximate compositional characteristics of the most primitive member E lavas. This compositional fit is far from perfect however, suggesting that petrogenesis of member E was substantially more complicated than a simple mixing model.

### MEMBER F

Member F lavas represent the final phase of magmatism of the MHVC, and while these rocks are andesites, they are compositionally distinct from the andesites of member E. At comparable MgO contents, member F lavas have less FeO and $TiO_2$ and represent evolved members of the calc-alkaline trend defined by members A and B. Unlike member E, which is andesitic to dacitic, the composition of member F is more primitive. Notwithstanding, these compositions suggest that member F flows may reflect a return to the style of magmatism that characterizes members A and B.

## THE MOUNT HARPER MELTING REGIME

In the following section we present the results of thermodynamic models aimed at understanding the evolution of the Mount Harper volcanic suite.

### MODELING THE LIQUID LINE OF DESCENT

Using alphaMELTS/pHMELTS (Asimow *et al.*, 2004; Ghiorso *et al.*, 2002; Ghiorso and Sack, 1995), it is possible to model the liquid line of descent (LLOD) starting from a parental melt composition. We approximate the parental melt using the Mount Harper sample with the highest MgO content. We have modeled the evolution of a parental melt composition (MgO = ~12%) during decreasing temperature over the pressure range of 1 to 20 kb, with water contents between 0 and 2%, and an oxygen fugacity buffered at FMQ-1 and FMQ.

Regardless of the temperature or oxygen fugacity buffer used, the anhydrous model runs all show enrichments in $FeO_T$ and $TiO_2$ with decreasing MgO, along with initial decreasing $SiO_2$ driven by the relatively early appearance of plagioclase on the liquidus. This tholeiitic (Fenner) trend is clearly incompatible with the observed LLOD for members A and B. The addition of water above 1% suppresses $FeO_T$ and $TiO_2$ enrichment as plagioclase crystallization is impeded.

Trends in both major element and normative compositions (Fig. 6) indicate that members A and B can be successfully

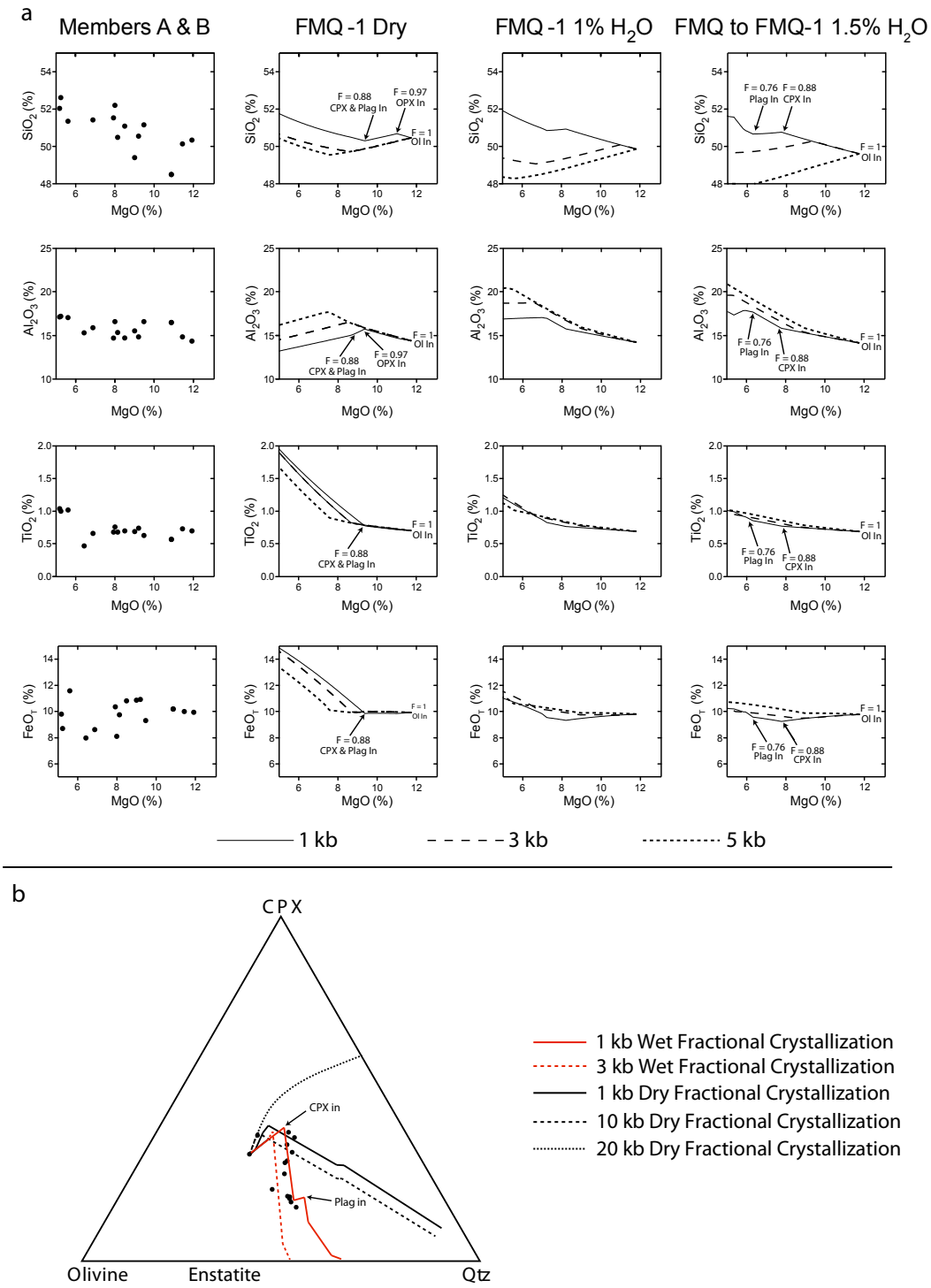


***Figure 6.*** *(a) Major element Fenner diagrams with modeled liquid lines of descent under varied oxygen fugacity constraints. These models demonstrate the requirement for a wet, low pressure melt to suppress the appearance of plagioclase on the liquidus. Such plagioclase suppression results in flat $FeO_T$ and $TiO_2$, as observed in members A and B. (b) Normative data projected onto the Ol-CPX-Qtz ternary diagram, modeling the liquid line of descent for wet and dry magmas under various pressure regimes. The data best fits that of a low pressure, wet melt. Based on these models, the compositional range observed for members A and B can be explained by the ~30% crystallization of Ol, followed by CPX, and then plagioclase. For fractional crystallization, the melt is held at constant pressure and cooled in increments of 1°C. As crystallization proceeds the solid is immediately removed from the remaining liquid.*

modeled by the low pressure (~1 kb) fractional crystallization of olivine followed by clinopyroxene. The entire compositional range of members A and B between ~12% to ~6% MgO requires approximately 30% fractional crystallization of a wet melt (1-1.5% $H_2O$) at FMQ-1 to FMQ conditions (Fig. 6a, right column).

These models have focused principally on understanding the petrogenesis of members A and B. However, they demonstrate that the range in composition in member E lavas is successfully modeled by fractionation of the most primitive member E lava (highest MgO%) under anhydrous and low $H_2O$ (*i.e.*, less than 0.5%) conditions. The trend observed for these lavas is compatible with fractionation of CPX+plagioclase of a relatively dry melt (Fig. 6a).

olivine and flags potential errors in the calculation caused by clinopyroxene fractionation or sources possibly characterized by carbonated peridotite and/or pyroxenite components.

The results of the two different approaches are shown in Table 1. There is broad agreement, with both methods calculating picritic primary melts with MgO contents between 14-17% MgO. Based on the calculated MgO contents of these parental melts, and using the equation for calculating mantle potential temperatures (Tp) as outlined by Herzberg *et al.* (2007), the calculated mantle potential temperature[1] for these melts lies between 1440°C and 1511°C , which is ~90°C to 160°C higher than inferred ambient mantle temperature (Herzberg *et al.*,

***Table 1.*** *Primary melt calculations.*

| | $SiO_2$ | $TiO_2$ | $Al_2O_3$ | $FeO_T$ | MnO | MgO | CaO | $Na_2O$ | $K_2O$ | $P_2O_5$ | Total | Liquidus T |
|---|---|---|---|---|---|---|---|---|---|---|---|---|
| Starting Composition | 50.14 | 0.73 | 14.84 | 9.97 | 0.19 | 11.45 | 12.09 | 0.21 | 0.13 | 0.07 | 100 | 1265 |

| Primary Melt | $SiO_2$ | $TiO_2$ | $Al_2O_3$ | $FeO_T$ | MnO | MgO | CaO | $Na_2O$ | $K_2O$ | $P_2O_5$ | Total | Olivine Fo | Tp | % Ol Addition |
|---|---|---|---|---|---|---|---|---|---|---|---|---|---|---|
| Method 1 - Fo90 | 49.47 | 0.68 | 13.69 | 10.16 | 0.18 | 14.31 | 11.18 | 0.19 | 0.12 | 0.06 | 100 | 90.0 | 1442 | 7.0 |
| Method 2 - PRIMELT2 | 48.70 | 0.62 | 12.59 | 9.17 | 0.94 | 17.17 | 10.28 | 0.18 | 0.11 | 0.06 | 100 | 91.3 | 1511 | 16.8 |

## PRIMARY MELT CALCULATIONS

The variation in $FeO_T$ on Figure 4 best demonstrates that samples of members A and B with MgO>9% have only fractionated olivine; this observation is supported by the melt modeling (Fig. 6), as discussed in the previous section. Such a simple fractionation pathway allows for the primary mantle melt to be reconstructed (as a melt in equilibrium with mantle olivine). Two methods have been applied to achieve this primary melt calculation. First, olivine is incrementally added back to the chosen parental melt composition until the liquid is in equilibrium with mantle olivine of ~$Fo_{90}$, using the FeO/MgO olivine-liquid distribution co-efficient ($K_D$) of 0.3 (Roeder and Emslie, 1970). Second, we apply the PRIMELT2 model of Herzberg and Asimow (2008), which couples the above inverse model with a forward melting model, such that the intersection of the two indicates the primary mantle melt. Unlike the first model, the PRIMELT2 method does not assume or require the Fo content of coexisting

2007). Of the two methods used, the PRIMELT2 method is preferred as it predicts a harzburgitic source (Fo91.3) which is the best fit for the most primitive lava combining the characteristics of low $TiO_2$, low $Al_2O_3$, and low $Na_2O$ (Falloon *et al.*, 1988).

With a reconstructed primary melt composition, critical melting regime characteristics can be evaluated such as percentage melting, melting depth, and source composition. The primary melt composition is projected onto modeled mantle melting curves in Figure 7. The principal variables that affect this calculation include oxygen fugacity, source composition, and pressure during melting (*i.e.*, specifically isobaric *vs.* polybaric path options). Oxygen fugacity is fixed to FMQ-1 based on the calculated fugacity of the Proterozoic upper mantle underlying the Canadian Cordillera as determined from

[1]*The mantle potential temperature (Tp) is the temperature the mantle would have at the earths surface if it ascended along an adiabat without undergoing melting (McKenzie and Bickle, 1988).*

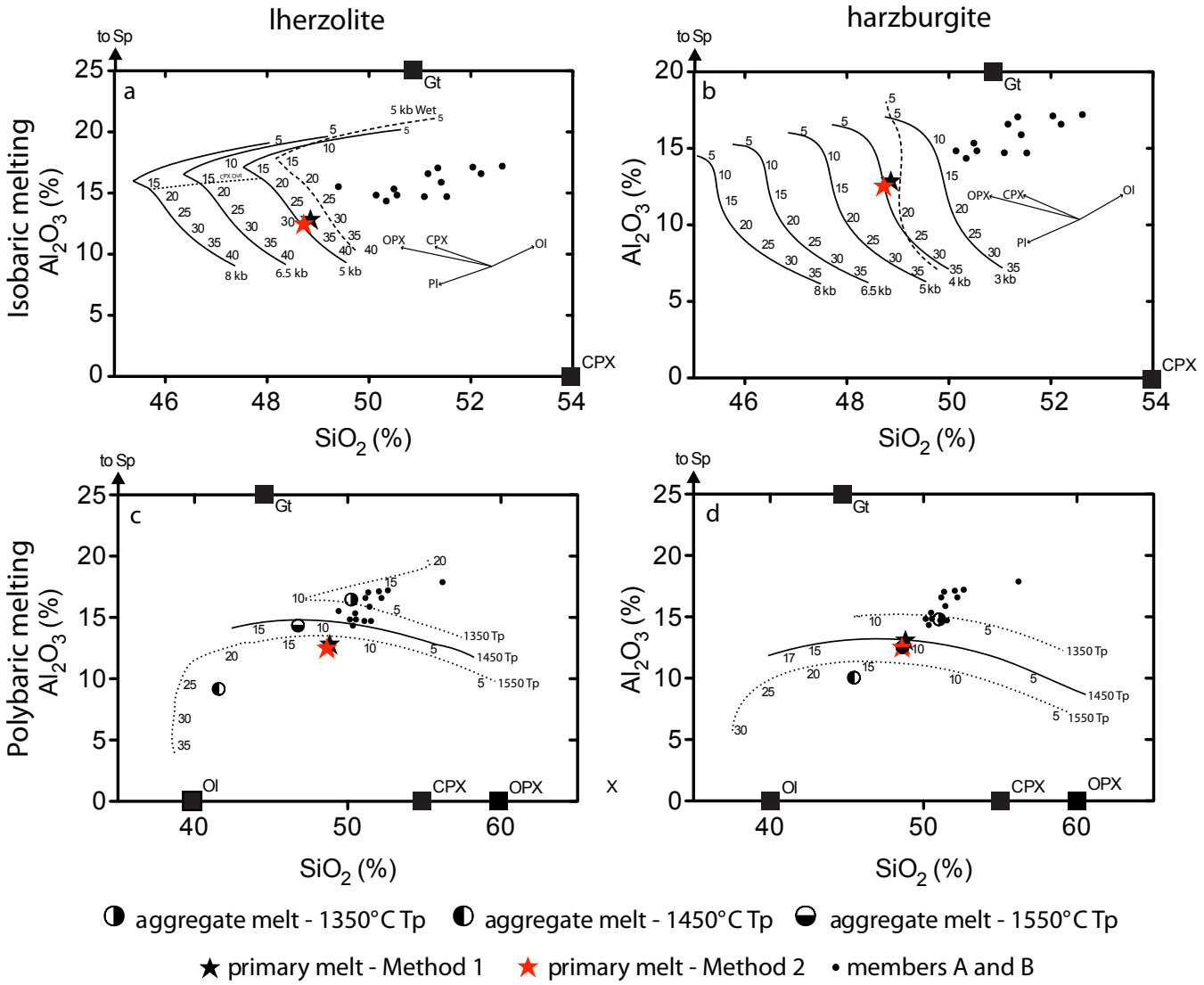


***Figure 7.*** *(a) Isobaric lherzolite melting (b) isobaric harzburgite melting (c) polybaric lherzolite melting (d) polybaric harzburgite melting. The numbers along the melting curves represent percentage melting. Normative minerals: CPX – clinopyroxene; Gt – garnet; Ol - olivine; OPX – orthopyroxene.*

mantle xenoliths (Francis *et al.*, 2010). The nature of the fertile mantle is semi-constrained using a lherzolitic composition as represented by the Kettle River peridotite (Walter, 1998), a sub-lithosphere mantle xenolith from British Columbia. The harzburgitic composition used in this calculation is that of Kettle River peridotite minus ~12% melt. Normative CPX compositions for the respective sources are 16% CPX for the lherzolite and 6% CPX for the harzburgite.

## OPTION 1: EQUILIBRIUM ISOBARIC MELTING

Calculated melting curves for a lherzolite source at pressures between 8 kb and 3 kb (24-9 km depth; Fig. 7) reveal that the primary melt composition requires an extraordinary high degree of partial melting (~30%), well past the CPX-out boundary at pressures of 5 kb. Modification of the source to a harzburgitic composition pushes the melting regime to even shallower levels (4 kb) and still requires melting to progress ~10% past the CPX-out boundary.

Several issues arise from these isobaric melting calculations. They imply high degrees of partial melting well beyond the thermal barrier represented by the Sp CPX-out phase boundary, require that the melt be generated entirely within what should be lithospheric mantle, and are based on isobaric mantle melting, which is a doubtful mantle melting process.

## OPTION 2: POLYBARIC ISENTROPIC MELTING

It has been shown that polybaric melting of an upwelling mantle source is a fractional melting process due to mantle compaction and the buoyancy of melt with respect to the mantle (Langmuir *et al.*, 1992; McKenzie and Bickle, 1988; McKenzie, 1984; Obata and Nagahara, 1987). Consequently, the fractionation of melt away from the mantle source results in mantle melting being largely isentropic in nature (Asimow *et al.*, 1995). This is more realistic for modeling mantle melting, and so we calculate the P-T path (Fig. 8), the percentage melt, instantaneous melt composition, and aggregate melt composition for both a lherzolite and harzburgite source, rising along adiabats that correspond to mantle potential temperatures of ~1350°C, ~1450°C, and ~1550°C (which bracket the calculated Tp of the primary melt). In the modeling runs, melting begins at the pressure where the corresponding mantle adiabat intersects the respective source solidus and continues up to the base of the lithosphere (which has been adjusted to be between 2 kb and 5 kb for this study (*i.e.*, ~6-15 km depth)).

Figure 7 shows that a lherzolite source is incompatible with the calculated primary melt as it consistently produces aggregate melts that are too high in $Al_2O_3$. The addition of water, which displaces these melting curves to higher $SiO_2$ as the peritectic in the Ol-CPX-Qtz ternary system moves towards the CPX-Qtz join, has very little effect on $Al_2O_3$ contents. The results for a harzburgitic source however show good agreement between the calculated primary melt and the aggregate melt generated by a rising mantle that begins to melt at ~17 kb (Fig. 8). Furthermore, the melt aggregation of this polybaric melting column, at ~2 kb, is consistent with the depth at which the modeled ~1 kb liquid line of descent from the most MgO-rich lava matches the natural variation observed in members A and B.

The largest source of uncertainty in this modeling exercise comes from source composition and the selected thickness of the lithosphere. However, by comparing variations in both the source composition and lithosphere thickness, we can gauge the sensitivity of the results to changes in these parameters.

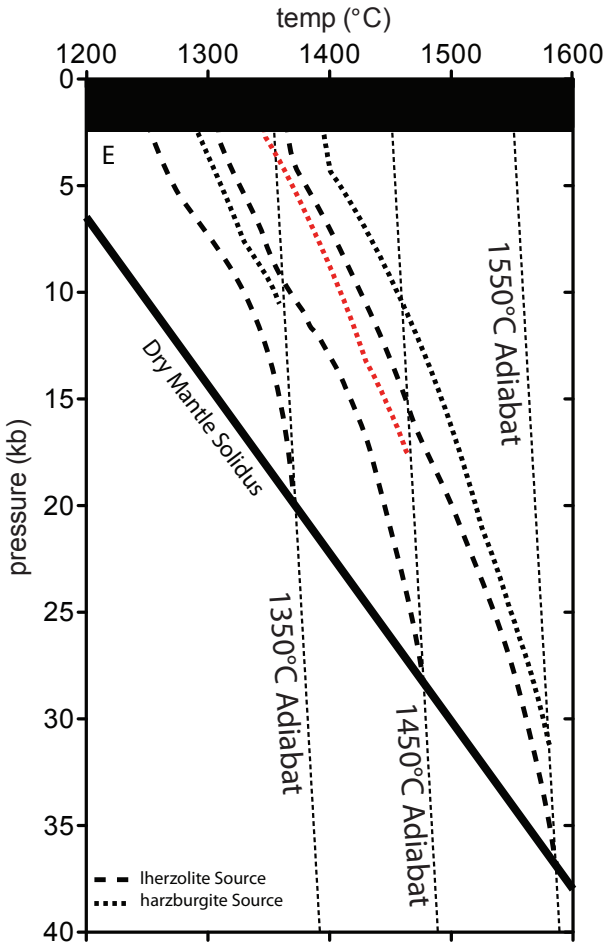


***Figure 8.*** *P/T diagram showing the melt path for the polybaric melting models. Solid black line is the dry solidus for lherzolite mantle (solidus for harzburgite is not shown, but would connect with the high pressure end of the harzburgite melting paths). Path shown in red is for a harzburgite source that intersects the solidus at ~17 kb along a 1450°C adiabat and successfully produces the primary melt composition calculated for members A and B. For the polybaric melting models, the source is maintained at a constant entropy state and melting proceeds under equilibrium conditions until the fraction of melt reaches F=0.005, at which point this melt is removed. The aggregate melt is the summation of these small equilibrium batch melts.*

It is evident from Figure 9 that the source composition has a larger impact on $Al_2O_3$ than $SiO_2$. This is not surprising, considering that Al is effectively incompatible during mantle melting (Falloon *et al.*, 1988). Unlike

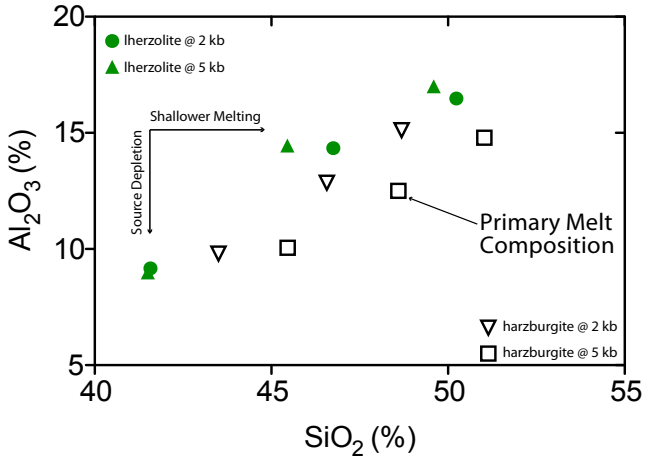


***Figure 9.*** *The effect of changes in source composition and depth to the crust/lithosphere boundary on the polybaric melting models and the effect this has on the ability to constrain these mantle melting parameters. It is evident that $SiO_2$ is primarily affected by pressure, while $Al_2O_3$ is affected by source composition, making these two variables independent proxies of these mantle melting variables.*

source composition, the thickness of the lithosphere and hence the pressure of melting has a large impact on $SiO_2$ and comparatively little impact on $Al_2O_3$. The increase in $SiO_2$ is readily explained by the shift of the peritectic and eutectic positions in the Ol-CPX-Qtz system to more $SiO_2$-rich compositions with decreasing pressure (Bowen and Schairer, 1935; Falloon *et al.*, 1988; Takahashi and Kushiro, 1983). Thus $Al_2O_3$ and $SiO_2$ compositions work as semi-independent constraints on the depth of melting and source composition. Other combinations of source composition and depth of the crust/lithosphere will not satisfy the primary melt composition at geologically reasonable mantle potential temperatures. Hence, these models place useful estimates on the melting regime and suggest polybaric melting of harzburgite beneath a lithosphere ~6 km thick (2 kb).

# DISCUSSION

## TECTONIC SETTING

The models presented here provide quantification of the melt that may have produced the initial volcanic accumulation at Mount Harper. They suggest that the melting that produced the MHVC was a direct result of mantle decompression to pressures of ~2 kb. This pressure implies that the overlying lithosphere was only ~6 km thick. Considering the average thickness of continental crust is ~39 km (Christensen and Mooney, 1995), combined with evidence for significant terrestrial (Lower Mount Harper Group) sedimentation, crustal attenuation by extension was well advanced when volcanism began, clearly pointing to a rift tectonic setting for the MHVC.

A modern analogue for continental transitioning to oceanic rift processes is the East-African-Red Sea-Gulf of Aden rift system. Seismic refraction profiles show significant variability in crustal/lithosphere thicknesses, from ~10 km at the flanks of the Red Sea which transitions to less than 6 km in the Gulf of Aden and the central Red Sea, while the less developed East Africa and Dead Sea rift arms have crustal thicknesses of ~20-30 km (Prodehl *et al.*, 1997). The calculated crustal thickness of ~6 km for the MHVC is consistent with the thickness of the off-axis regions of the Red Sea. While the Red Sea is dominated by a central spreading ridge, many seamounts and volcanic islands can be found along the full length of the central rift (Gass *et al.*, 1973), as well as volcanic centres that flank and onlap onto the coastal zones (*i.e.*, Wiart and Oppenheimer, 2000). Mustard and Roots (1997) originally proposed an East-African rift analogy with incipient low-angle normal faults (Bosworth, 1985). Based on our calculations for the thickness of the lithosphere a more evolved rift setting is appropriate.

## A FAR-FLUNG COMPONENT OF THE FRANKLIN LIP?

The Franklin Igneous Province was a LIP manifested by a dike swarm radiating 2500 km across northern Canada and Greenland (Dawes, 1992; Denyszyn *et al.*, 2009; Frisch, 1984a,b,c) and the Natkusiak basalts of Victoria Island (Dostal *et al.*, 1986) at ~720 Ma (Denyszyn *et al.*, 2009; Heaman *et al.*, 1992). The age of the rhyolite (subsequent to members A and B) at MHVC is the same age as the Franklin LIP which leads to conjecture that the MHVC could be part of the Franklin Igneous Province.

The published major element data of Dostal *et al.* (1986) and Denyszyn (2008) show fundamental geochemical differences between the MHVC and Franklin extrusive and intrusive occurrences (Fig. 10). Specifically, Franklin igneous rocks are more evolved, lying along a gabbroic fractionation trend. Additionally, $TiO_2$ and FeO enrichments indicate a clear tholeiitic evolution in the Franklin volcanics, in contrast to the calc-alkaline evolution of the MHVC.

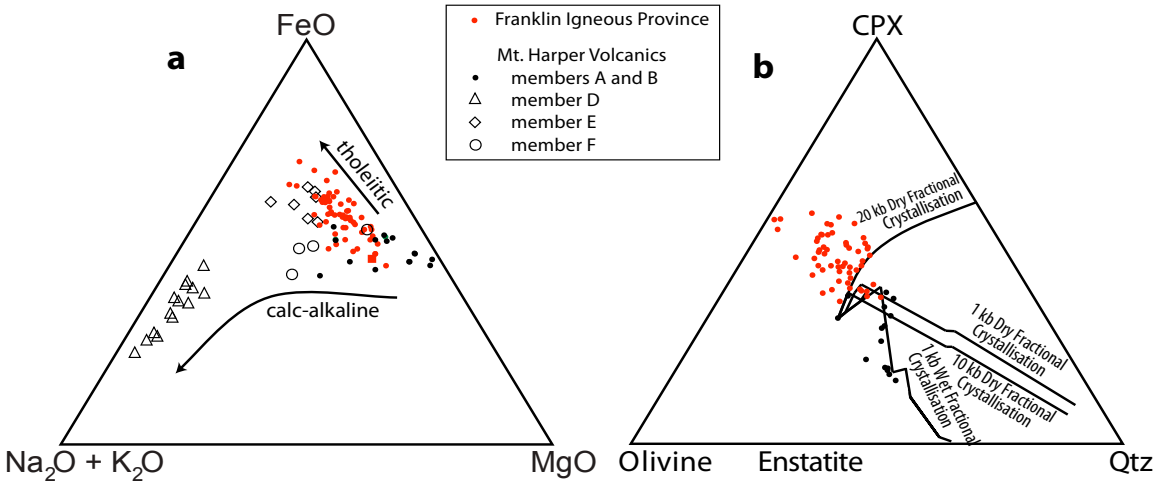


***Figure 10.*** *(a) AFM diagram showing a comparison between major element data for the Franklin LIP in red (Dostal et al., 1986; Denyszyn, 2008), along with our data for the MHVC (black). The Franklin rocks evolved along a tholeiitic pathway, whereas MHVC define a calc-alkaline trajectory. (b) Normative compositions for the Franklin igneous rocks (red) reveal a trend associated with the fractionation of a dry magma from a parental melt, significantly different from the parental melt for members A and B of the MHVC (black). The trend exhibited by the Franklin igneous rocks are similar to that obtained experimentally for fractionation of a basaltic liquid in equilibrium with a lherzolite residue (Villiger et al., 2004).*

This comparison is explored by examining the volcanic suites at similar stages in their evolution. The data sets are normalized to a common MgO% to correct for the effects of fractionation, following the method outlined by Klein and Langmuir (1987). This analysis (Table 2) reveals that, at comparable stages, the MHVC are shifted to higher $SiO_2$, lower $TiO_2$, lower FeO, lower CaO, and lower $Na_2O$. These systematic shifts indicate completely different sources, reinforcing the deduction that the Natkusiak basalts are lherzolite melts (Falloon *et al.*, 1988; Klein and Langmuir, 1987; Turner and Hawkesworth, 1995), whereas the MHVC are harzburgite melts (Falloon *et al.*, 1988; Turner and Hawkesworth, 1995). This conclusion concerning different mantle sources agrees with that reached by Dostal *et al.* (1986), who argued that an N-MORB type source best suited the Natkusiak basalts and our modeling of the MHVC.

***Table 2.*** *Major element values for the Mount Harper Volcanic Complex and Nakusiak basalts corrected to a common value of MgO equals 8% (after Klein and Langmuir, 1987).*

| | $Si_{8.0}$ | $Ti_{8.0}$ | $Al_{8.0}$ | $Fe_{8.0}$ | $Mn_{8.0}$ | $Ca_{8.0}$ | $Na_{8.0}$ | $K_{8.0}$ | $P_{8.0}$ |
|---|---|---|---|---|---|---|---|---|---|
| Nakusiak Basalts | 50.27 | 1.40 | 14.12 | 12.10 | 0.20 | 11.01 | 2.21 | 0.52 | 0.17 |
| MHVC | 51.89 | 0.73 | 15.99 | 9.80 | 0.18 | 10.57 | 2.11 | 0.50 | 0.08 |

Systematic differences between the MHVC and Franklin igneous rocks indicate that melt was generated from distinct mantle reservoirs under different conditions. This does not preclude a link between the MHVC and the Franklin volcanics however, if both are considered in the broader context of a plume model proposed for the emplacement of LIP's (Campbell, 2005; Sobolev *et al.*, 2011). The combination of a large radiating dike swarm, high pressure melting (garnet residue; Dostal *et al.*, 1986) and continental doming that preceded the eruption of the Natkusiak basalts (Rainbird, 1993) are consistent with a plume source for the Franklin LIP. A possible plume source for the MHVC is suggested by our calculation of mantle potential temperatures that are 90°C to 160°C above ambient mantle (Herzberg *et al.*, 2007). However, it has been recognized that elevated mantle potential temperatures need not require rising hot asthenosphere, because modeling results suggest that continental insulation can produce an increase in mantle temperatures of at least ~100°C (Anderson, 1982; Coltice *et al.*, 2007; Grigne and Labrosse, 2001). Consequently, the higher mantle potential temperatures calculated for the MHVC are equally compatible with mantle insulation and mantle plume models (Campbell and Griffiths, 1990; Herzberg *et al.*, 2007; Watson and McKenzie, 1991).

An alternative explanation for the discrepancy between the MHVC and the Franklin LIP (Heaman *et al.*, 1992; Rainbird, 1993) may lie in the geographic distance between them and the harzburgitic source required for the MHVC. The thermochemical plume model (Campbell, 2007; Campbell and Griffiths, 1990; Griffiths and Campbell, 1990; Watson and McKenzie, 1991; Wyllie, 1988) posits that hot, adiabatically decompressing mantle impinges on the base of the lithosphere and flattens. Most melting should occur in the rising plume, leaving a melt-depleted mantle that flows radially away from the plume centre along the base of the lithosphere. Consequently a harzburgitic residue related to the Franklin plume might conceivably be the source of the MHVC at the "far flung" fringe of the flattened plume head.

## CONCLUSIONS

The composition of igneous rocks of the MHVC can be modeled by polybaric melting of a mantle harzburgite source. The liquid line of descent of this melt would have followed a calc-alkaline differentiation trend characterized by low pressure fractionation of olivine ± clinopyroxene and the delayed appearance of plagioclase. Calculated primary melt composition requires mantle temperatures above those considered normal for the ambient mantle.

This volcanic complex represents a dominantly sub-aqueous magmatic episode, interrupted by a minor interlude of sub-aerial volcanic activity. It would suggest a volcanic island developed in a rift setting, possibly analogous to fringes of the modern Red Sea.

Although the identical ages between the MHVC and the Franklin LIP suggest a synchronous origin for the two, their inferred sources were different. Only by differentiation of a mantle plume as it spread radially, then tapped by a half-graben fault through thinned continental crust, could the MHVC be related to the Franklin Large Igneous Province.

## ACKNOWLEDGMENTS

This project has been supported by Yukon Geological Survey and NSERC grants to GPH and a Vanier Fellowship to GMC. Don Francis is thanked for many helpful discussions. Bill Horne re-drafted some figures. This is ESS Contribution number 20120369.

## REFERENCES

Anderson, D.L., 1982. Hotspots, polar wander, Mesozoic convection and the geoid. Nature, vol. 297, p. 391-393.

Asimow, P.D., Dixon, J.E., and Langmuir, C.H., 2004. A hydrous melting and fractionation model for mid-ocean ridge basalts: Application to the Mid-Atlantic Ridge near the Azores. Geochemistry, Geophysics, Geosystems, vol. 5, p. Q01E16.

Asimow, P.D., Hirschmann, M.M., Ghiorso, M.S., O'Hara, M.J., and Stolper, E.M., 1995. The effect of pressure-induced solid-solid phase transitions on decompression melting of the mantle. Geochimica et Cosmochimica Acta, vol. 59, p. 4489-4506.

Blundy, J. and Cashman, K., 2001. Ascent-driven crystallisation of dacite magmas at Mount St Helens, 1980-1986. Contributions to Mineralogy and Petrology, vol. 140, p. 631-650.

Bosworth, W., 1985. Geometry of propagating continental rifts. Nature, vol. 316, p. 625-627.

Bowen, N.L. and Schairer, J.F., 1935. The system MgO-FeO-$SiO_2$. American Journal of Science, Series 5, vol. 29, p. 151-217.

Campbell, I.H., 2005. Large Igneous Provinces and the Mantle Plume Hypothesis. Elements, vol. 1, p. 265-269.

Campbell, I.H, 2007. Testing the plume theory. Chemical Geology, vol. 241, p. 153-176.

Campbell, I.H. and Griffiths, R.W., 1990. Implications of mantle plume structure for the evolution of flood basalts. Earth and Planetary Science Letters, vol. 99, p. 79-93.

Chappell, B.W. and White, A.J.R., 2001. Two contrasting granite types: 25 years later. Australian Journal of Earth Sciences, vol. 48, p. 489-499.

Christensen, N.I. and Mooney, W.D., 1995. Seismic velocity structure and composition of the continental crust: A global view. Journal of Geophysical Research, vol. 100, p. 9761-9788.

Coltice, N., Phillips, B.R., Bertrand, H., Ricard, Y., and Rey, P., 2007. Global warming of the mantle at the origin of flood basalts over supercontinents. Geology, vol. 35, p. 391-394.

Dalziel, I.W.D., Lawver, L.A., and Murphy, J.B., 2000. Plumes, orogenesis, and supercontinental fragmentation. Earth and Planetary Science Letters, vol. 178, p. 1-11.

Dawes, D.W., 1992. Geological compilation map of the Thule area, Greenland. Geological Survey of Greenland, scale 1:500 000.

Denyszyn, S.W., 2008. Paleomagnetism, geochemistry and U-Pb geochronology of Proterozoic mafic intrusions in the High Arctic: Relevance to the Nares Strait problem. PhD dissertation, University of Toronto.

Denyszyn, S.W., Halls, H.C., Davis, D.W., and Evans, D.A.D., 2009. Paleomagnetism and U-Pb geochronology of Franklin dykes in High Artic Canada and Greenland: a revised age and paleomagnetic pole constraining block rotations in the Nares Strait region. Canadian Journal of Earth Sciences, vol. 46, p. 689-705.

Dostal, J., Baragar, W.R.A., and Dupuy, C., 1986. Petrogenesis of the Natkusiak continental basalts, Victoria Island, Northwest Territories, Canada. Canadian Journal of Earth Sciences, vol. 23, p. 622-632.

Ernst, R.E. and Buchan, K.L., 1997. Giant radiating dyke swarms: Their use in identifying pre-Mesozoic large igneous provinces and mantle plumes. *In:* Large Igneous Provinces: Continental, Oceanic, and Planetary Flood Volcanism, J.J. Mahoney and M.F. Coffin (eds.), American Geophysical Union, Washington.

Ernst, R.E. and Buchan, K.L., 2001. The use of mafic dike swarms in identifying and locating mantle plumes. Geological Society of America, Special Papers, vol. 352, p. 247-265.

Ernst, R.E. and Buchan, K.L., 2003. Recognizing mantle plumes in the geological record. Annual Review of Earth and Planetary Sciences, vol. 31, p. 469-523.

Falloon, T.J., Green, D.H., Hatton, C.J., and Harris, K.L., 1988. Anhydrous Partial Melting of a Fertile and Depleted Peridotite from 2 to 30 kb and Application to Basalt Petrogenesis. Journal of Petrology, vol. 29, p. 1257-1282.

Francis, D., Minarik, W., Proenza, Y., and Shi, L., 2010. An overview of the Canadian Cordilleran lithospheric mantle. Canadian Journal of Earth Sciences, vol. 47, p. 353-368.

Frisch, T., 1984a. Geology, Devon Ice Cap, District of Franklin, Northwest Territories. Geological Survey of Canada, scale 1:250 000.

Frisch, T., 1984b. Geology, Mackinson Inlet, District of Franklin, Northwest Territories. Geological Survey of Canada, scale 1:250 000.

Frisch, T., 1984c. Geology, Prince of Wales Mountains, District of Franklin, Northwest Territories. Geological Survey of Canada, scale 1:250 000.

Gass, I.G., Mallick, D.I.J., and Cox, K.G., 1973. Volcanic islands of the Red Sea. Journal of the Geological Society, vol. 129, p. 275-309.

Ghiorso, M.S. and Sack, R.O., 1995. Chemical mass transfer in magmatic processes IV. A revised and internally consistent thermodynamic model for the interpolation and extrapolation of liquid-solid equilibria in magmatic systems at elevated temperatures and pressures. Contributions to Mineralogy and Petrology, vol. 119, p. 197-212.

Ghiorso, M.S., Hirschmann, M.M., Reiners, P.W., and Kress III, V.C., 2002. The pMELTS: A revision of MELTS for improved calculation of phase relations and major element partitioning related to partial melting of the mantle to
3 GPa. Geochemistry, Geophysics, Geosystems, vol. 3, p. 1030.

Griffiths, R.W. and Campbell, I.H., 1990. Stirring and structure in mantle starting plumes. Earth and Planetary Science Letters, vol. 99, p. 66-78.

Grigne, C. and Labrosse, S., 2001. Effects of continents on Earth cooling: Thermal blanketing and depletion in radioactive elements. Geophysical Research. Letters, vol. 28, p. 2707-2710.

Harlan, S.S., Heaman, L., LeCheminant, A.N., and Premo, W.R., 2003. Gunbarrel mafic magmatic event: A key 780 Ma time marker for Rodinia plate reconstructions. Geology, vol. 31, p. 1053-1056.

Heaman, L.M., LeCheminant, A.N., and Rainbird, R.H., 1992. Nature and timing of Franklin igneous events, Canada: Implications for a Late Proterozoic mantle plume and the break-up of Laurentia. Earth and Planetary Science Letters, vol. 109, p. 117-131.

Herzberg, C. and Asimow, P.D., 2008. Petrology of some oceanic island basalts: PRIMELT2.XLS software for primary magma calculation. Geochemistry, Geophysics, Geosystems, vol. 9, p. Q09001.

Herzberg, C., Asimow, P.D., Arndt, N., Niu, Y., Lesher, C.M., Fitton, J.G., Cheadle, M.J., and Saunders, A.D., 2007. Temperatures in ambient mantle and plumes: Constraints from basalts, picrites, and komatiites. Geochemistry, Geophysics, Geosystems, vol. 8, p. Q02006.

Hill, R.I., 1991. Starting plumes and continental break-up. Earth and Planetary Science Letters, vol. 104, p. 398-416.

Klein, E.M. and Langmuir, C.H., 1987. Global Correlations of Ocean Ridge Basalt Chemistry with Axial Depth and Crustal Thickness. Journal of Geophysical Research, vol. 92, p. 8089-8115.

Langmuir, C.H., Klein, E.M., and Plank, T., 1992. Petrological systematics of mid-ocean ridge basalts: Constraints on melt generation beneath ocean ridges, in Mantle Flow and Melt Generation at Mid-Ocean Ridges. AGU Geophysical Monogragh Series, vol. 71, p. 183-280.

Li, Z.X., Kinny, P.D., Wang, J., Zhang, S., and Zhou, H., 2003. Geochronology of Neoproterozoic syn-rift magmatism in the Yangtze Craton, South China and correlations with other continents: evidence for a mantle superplume that broke up Rodinia. Precambrian Research, vol. 122, p. 85-109.

Macdonald, F.A., Halverson, G.P., Strauss, J.V., Smith, E.F., Cox, G.M., Sperling, E.A., and Roots, C.F., 2012. Early Neoproterozoic Basin Formation in Yukon, Canada: Implications for the make-up and break-up of Rodinia. Geoscience Canada, vol. 39, p. 77-99.

Macdonald, F.A., Schmitz, M.D., Crowley, J.L., Roots, C.F., Jones, D.S., Maloof, A.C., Strauss, J.V., Cohen, P.A., Johnston, D.T., and Schrag, D.P., 2010. Calibrating the Cryogenian. Science, vol. 327, p. 1241-1243.

Macdonald, F.A., Smith, E.F., Strauss, J.V., Cox, G.M., Halverson, G.P., and Roots, C.F., 2011. Neoproterozoic and early Paleozoic correlations in the western Ogilvie Mountains. *In:* Yukon Exploration and Geology 2010, K.E. MacFarlane, L.H. Weston, and C. Relf (eds.), Yukon Geological Survey, p. 161-182.

McHone, J.G., Anderson, D.L., Beutel, E.K., and Fialko, Y.A., 2005. Giant dikes, rifts, flood basalts, and plate tectonics: A contention of mantle models. Geological Society of America Special Papers, vol. 388, p. 401-420.

McKenzie, D.A.N., 1984. The Generation and Compaction of Partially Molten Rock. Journal of Petrology, vol. 25, p. 713-765.

McKenzie, D. and Bickle, M.J., 1988. The Volume and Composition of Melt Generated by Extension of the Lithosphere. Journal of Petrology, vol. 29, p. 625-679.

Mustard, P.S., 1991. Normal faulting and alluvial-fan deposition, basal Windermere Tectonic Assemblage, Yukon, Canada. Geological Society of America Bulletin, vol. 103, p. 1346-1364.

Mustard, P.S. and Donaldson, J.A., 1990. Paleokarst breccias, calcretes, silcretes and fault talus breccias at the base of upper Proterozoic "Windermere" strata, northern Canadian Cordillera. Journal of Sedimentary Research, vol. 60, p. 525-539.

Mustard, P.S. and Roots, C.F., 1997. Rift-related volcanism, sedimentation, and tectonic setting of the Mount Harper Group, Ogilvie Mountains, Yukon Territory. Geological Survey of Canada, Bulletin 492.

Obata, M. and Nagahara, N., 1987. Layering of Alpine-Type Peridotite and the Segregation of Partial Melt in the Upper Mantle. Journal of Geophysical Research, vol. 92, p. 3467-3474.

Prodehl, C., Fuchs, K., and Mechie, J., 1997. Seismic-refraction studies of the Afro-Arabian rift system — a brief review. Tectonophysics, vol. 278, p. 1-13.

Rainbird, R.H., 1993. The Sedimentary Record of Mantle Plume Uplift Preceding Eruption of the Neoproterozoic Natkusiak Flood Basalt. The Journal of Geology, vol. 101, p. 305-318.

Roeder, P.L. and Emslie, R.F., 1970. Olivine-liquid equilibrium. Contributions to Mineralogy and Petrology, vol. 29, p. 275-289.

Roots, C.F., 1987. Regional tectonic setting and the evolution of the Late Proterozoic Mount Harper volcanic complex, Ogilvie Mountains, Yukon. Doctoral dissertation, Carleton University, Ottawa, Ontario, 180 p.

Sobolev, S.V., Sobolev, A.V., Kuzmin, D.V., Krivolutskaya, N.A., Petrunin, A.G., Arndt, N.T., Radko, V.A., and Vasiliev, Y.R., 2011. Linking mantle plumes, large igneous provinces and environmental catastrophes. Nature, vol. 477, p. 312-316.

Storey, B.C., 1995. The role of mantle plumes in continental breakup: case histories from Gondwanaland. Nature, vol. 377, p. 301-308.

Takahashi, E. and Kushiro, I., 1983. Melting of a dry peridotite at high pressures and basalt magma genesis. American Mineralogist, vol. 68, p. 859-879.

Thompson, B., Mercier, E., and Roots, C., 1987. Extension and its influence on Canadian Cordilleran passive-margin evolution. Geological Society, London, Special Publications, vol. 28, p. 409-417.

Tosca, N.J., Macdonald, F.A., Strauss, J.V., Johnston, D.T., and Knoll, A.H., 2011. Sedimentary talc in Neoproterozoic carbonate successions. Earth and Planetary Science Letters, vol. 306, p. 11-22.

Turner, S. and Hawkesworth, C., 1995. The nature of the sub-continental mantle: constraints from the major-element composition of continental flood basalts. Chemical Geology, vol. 120, p. 295-314.

Villiger, S., Ulmer, P., Müntener, O., and Thompson, A.B., 2004. The Liquid Line of Descent of Anhydrous, Mantle-Derived, Tholeiitic Liquids by Fractional and Equilibrium Crystallization—an Experimental Study at 1·0 GPa. Journal of Petrology, vol. 45, p. 2369-2388.

Walter, M.J., 1998. Melting of Garnet Peridotite and the Origin of Komatiite and Depleted Lithosphere. Journal of Petrology, vol. 39, p. 29-60.

Watson, S. and McKenzie, D.A.N., 1991. Melt Generation by Plumes: A Study of Hawaiian Volcanism. Journal of Petrology, vol. 32, p. 501-537.

Wiart, P. and Oppenheimer, C., 2000. Largest known historical eruption in Africa: Dubbi volcano, Eritrea, 1861. Geology, vol. 28, p. 291-294.

Wyllie, P.J., 1988. Solidus Curves, Mantle Plumes, and Magma Generation Beneath Hawaii. Journal of Geophysical Research, vol. 93, p. 4171-4181.

# APPENDIX 1:

***Table S1.*** *New* major element data for the volcanic rocks of the Mount Harper volcanic complex.*

| Sample # | MH10-005 | MH10-033 | MH10-019 | MH10-026 | MH10-027 | MH10-447 | MH10-448 | MH10-034 | MH10-035 | MH10-036 | MH10-047 | MH10-051 | MH10-052B | MH10-054 | MH10-059 | MH10-071 | MH10-072 | MH10-064 |
|---|---|---|---|---|---|---|---|---|---|---|---|---|---|---|---|---|---|---|
| Member | A | A | B | B | B | B | B | D | D | D | D | D | D | D | D | E | E | F |
| $SiO_2$ | 51.35 | 49.4 | 62.18 | 52.62 | 52.04 | 51.53 | 51.09 | 71.27 | 72.41 | 72.73 | 78.37 | 72.63 | 70.96 | 74.14 | 74.09 | 58.71 | 59.01 | 56.79 |
| $TiO_2$ | 1.02 | 0.69 | 0.47 | 1.00 | 1.04 | 0.68 | 0.7 | 0.52 | 0.48 | 0.49 | 0.4 | 0.5 | 0.5 | 0.41 | 0.49 | 1.37 | 1.34 | 0.73 |
| $Al_2O_3$ | 17.06 | 15.53 | 15.3 | 17.21 | 17.13 | 14.71 | 14.72 | 13.5 | 13.16 | 13.19 | 10.03 | 13.43 | 13.27 | 10.77 | 12.82 | 13.76 | 13.7 | 15.58 |
| $Fe_2O_3$ | 1.95 | 1.83 | 1.34 | 1.46 | 1.65 | 1.74 | 1.82 | 0.69 | 0.75 | 0.71 | 0.43 | 0.42 | 0.76 | 0.7 | 0.48 | 1.84 | 1.87 | 1.31 |
| FeO | 9.8 | 9.19 | 6.74 | 7.36 | 8.29 | 8.76 | 9.15 | 3.45 | 3.78 | 3.58 | 2.15 | 2.12 | 3.82 | 3.53 | 2.42 | 9.27 | 9.39 | 6.58 |
| FeOT | 11.55 | 10.84 | 7.95 | 8.67 | 9.77 | 10.33 | 10.79 | 4.07 | 4.45 | 4.22 | 2.54 | 2.50 | 4.50 | 4.16 | 2.85 | 10.93 | 11.07 | 7.76 |
| MnO | 0.18 | 0.2 | 0.07 | 0.17 | 0.18 | 0.18 | 0.18 | 0.03 | 0.03 | 0.03 | 0.02 | 0.05 | 0.09 | 0.09 | 0.07 | 0.2 | 0.2 | 0.13 |
| MgO | 5.61 | 9.01 | 6.43 | 5.24 | 5.18 | 7.93 | 8.5 | 0.76 | 0.62 | 1.04 | 0.46 | 0.4 | 0.64 | 1.21 | 0.58 | 3.28 | 4.45 | 4.81 |
| CaO | 9.91 | 11.63 | 2.18 | 11.59 | 11.2 | 12.22 | 12.02 | 1.77 | 1.26 | 1.15 | 1.06 | 2.19 | 3.5 | 3.1 | 1.77 | 7.07 | 5.36 | 8.05 |
| $Na_2O$ | 2.22 | 2.13 | 4.29 | 2.18 | 2.15 | 1.62 | 1.49 | 0.27 | 1.31 | 0.17 | 0.43 | 2.03 | 0.38 | 1.32 | 0.4 | 1.53 | 1.75 | 4.32 |
| $K_2O$ | 0.62 | 0.36 | 0.95 | 1.04 | 1.02 | 0.55 | 0.26 | 7.54 | 6.02 | 6.7 | 6.53 | 6.03 | 5.89 | 4.58 | 6.73 | 2.69 | 2.64 | 1.58 |
| $P_2O_5$ | 0.27 | 0.05 | 0.06 | 0.12 | 0.13 | 0.08 | 0.08 | 0.2 | 0.2 | 0.21 | 0.12 | 0.19 | 0.19 | 0.14 | 0.15 | 0.29 | 0.28 | 0.12 |
| Total | 100 | 100 | 100 | 100 | 100 | 100 | 100 | 100 | 100 | 100 | 100 | 100 | 100 | 100 | 100 | 100 | 100 | 100 |
| LOI | 4.18 | 2.78 | 4.61 | 4.85 | 4.72 | 2.41 | 2.87 | 3.12 | 2.46 | 2.84 | 1.98 | 2.69 | 4.55 | 4.17 | 2.99 | 3.32 | 3.52 | 5.73 |
| Normative Minerology | | | | | | | | | | | | | | | | | | |
| Q | 3.11 | 0.00 | 14.67 | 3.54 | 3.05 | 2.14 | 2.34 | 34.23 | 36.14 | 40.30 | 46.91 | 31.72 | 35.68 | 39.41 | 40.24 | 16.35 | 15.75 | 1.43 |
| or | 3.66 | 2.13 | 5.61 | 6.15 | 6.03 | 3.25 | 1.54 | 44.56 | 35.57 | 39.60 | 38.59 | 35.64 | 34.81 | 27.07 | 39.77 | 15.90 | 15.60 | 9.34 |
| ab | 18.79 | 18.02 | 36.30 | 18.45 | 18.19 | 13.71 | 12.61 | 2.28 | 11.08 | 1.44 | 3.64 | 17.18 | 3.22 | 11.17 | 3.38 | 12.95 | 14.81 | 36.56 |
| an | 34.76 | 31.75 | 10.42 | 34.11 | 34.08 | 31.24 | 32.71 | 7.47 | 4.94 | 4.33 | 4.47 | 9.62 | 16.12 | 9.94 | 7.80 | 22.73 | 21.73 | 18.45 |
| C | 0.00 | 0.00 | 3.39 | 0.00 | 0.00 | 0.00 | 0.00 | 2.16 | 2.68 | 4.07 | 0.61 | 0.04 | 0.36 | 0.00 | 2.02 | 0.00 | 0.00 | 0.00 |
| di | 10.49 | 20.90 | 0.00 | 18.60 | 17.05 | 23.60 | 21.57 | 0.00 | 0.00 | 0.00 | 0.00 | 0.00 | 0.00 | 3.82 | 0.00 | 8.79 | 2.53 | 17.03 |
| hy | 23.80 | 13.21 | 26.64 | 14.87 | 16.94 | 22.06 | 25.09 | 6.86 | 7.13 | 7.82 | 4.12 | 3.81 | 7.32 | 6.48 | 4.81 | 17.35 | 23.68 | 13.63 |
| ol | 0.00 | 9.93 | 0.00 | 0.00 | 0.00 | 0.00 | 0.00 | 0.00 | 0.00 | 0.00 | 0.00 | 0.00 | 0.00 | 0.00 | 0.00 | 0.00 | 0.00 | 0.00 |
| mt | 2.83 | 2.65 | 1.94 | 2.12 | 2.39 | 2.52 | 2.64 | 1.00 | 1.09 | 1.03 | 0.62 | 0.61 | 1.10 | 1.02 | 0.70 | 2.67 | 2.71 | 1.90 |
| il | 1.94 | 1.31 | 0.89 | 1.90 | 1.98 | 1.29 | 1.33 | 0.99 | 0.91 | 0.93 | 0.76 | 0.95 | 0.95 | 0.78 | 0.93 | 2.60 | 2.55 | 1.39 |
| ap | 0.63 | 0.12 | 0.14 | 0.28 | 0.30 | 0.19 | 0.19 | 0.46 | 0.46 | 0.49 | 0.28 | 0.44 | 0.44 | 0.32 | 0.35 | 0.67 | 0.65 | 0.28 |

*For results described in this paper, these were combined with data from Mustard and Roots (1997). From this previous work, the following samples were used:

Member A: 127-2, 128-3; Member B: 97a, 118-3, 126-2, 128-15, 129-0, 158-1, 158-2, 162-1.

Member D: 44, 48-1, 103, 138-1, 138-2, 138-3, 138-4, 154, 166; Member E: 72-2, 79-1, 82-4, 99, 144-6; Member F: 121-7; 161

**Analytic methods:**

Rock samples were first trimmed to remove weathered surfaces and then cut into ~5 $cm^3$ fragments using a diamond-bladed rock saw. The rocks were crushed to rock chips on a iron jaw crusher. The chips where milled in a hardened steel mill until the powder could pass through a 75 µm mesh. Major and trace element abundances were analysed by X-ray fluorescence using a Philips PW2400 4kW automated XRF spectrometer system with a rhodium 60 kV end window X-ray tube. Major elements, Cr, Ni, and V were analysed using 32 mm diameter fused beads prepared from a 1:5 sample/lithium tetraborate mixture. Sc, Rb, Sr, Zr, Nb, and Y were analysed using 40 mm diameter pressed pellets prepared at a pressure of 20 tonnes from a mixture of 10 g sample powder with 2 g Hoechst Wax C Micropowder. Calibration regression lines were prepared using between 15 and 40 International Standard Reference Materials. Corrections for mass absorption effects were applied on concentration values using a combination of alpha coefficients and/or Compton scatter. The accuracy for silica is within 0.5% absolute, 1% for other majors, and within 5% for trace elements. Instrument precision is within 0.3% relative, generally within 0.23% relative, and the overall precision for beads and pressed pellets is within 0.5% relative.